Available online at www.sciencedirect.com

ScienceDirect

IFAC Papers Online CONFERENCE PAPER ARCHIVE

IFAC-PapersOnLine 48-9 (2015) 079–084

Fully Actuated Tricopter with Pilot-Supporting Control ⋆

D. Kastelan, M. Konz, J. Rudolph

Chair of Systems Theory and Control Engineering,
Saarland University, Campus A5 1, 66123 Saarbrücken, Germany.
d.kastelan/m.konz/j.rudolph@lsr.uni-saarland.de

Abstract: A tricopter with three tilting motor-supporting arms in a planar $2\pi/3$-distributed configuration is investigated. A single rigid body approximate model thereof is shown to be fully actuated, thus allowing for a variety of flight maneuvers including translation without tilting and inclined hovering. A pilot-supporting control strategy is presented consisting of two parts: a nonlinear attitude tracking controller based on a rotation matrix attitude parametrization; and a heading-referenced acceleration command generator. Together these allow the pilot to intuitively command vehicle motions for a chosen tilted body configuration. The construction of the vehicle is discussed and experimental flight results show good attitude controller performance.

Keywords: UAV, attitude control, nonlinear control, vehicle dynamics, aerodynamics.

1. INTRODUCTION

Small unmanned aerial vehicles (UAVs) have proven themselves to be an ongoing topic of great research interest, given their promise as extremely versatile sensing and transport platforms. A recent review thereof, along with related opportunities and challenges, is provided by Kumar and Michael (2012). For indoor and short-range applications, vehicle designs have all but converged on the so-called multicopter arrangement of direct-drive fixed-pitch propellers that provide the forces and torques necessary for stabilization and navigation in three-dimensional space.

Typically, these actuators are introduced pairwise, such that inherent aerodynamic reaction torques cancel in the nominal hover case through the use of counter-rotating propellers. Furthermore, their orientations with respect to the vehicle frame are usually fixed in the vertical direction, as to maximize weight-countering thrust in hover. The results are mechanically simple and robust vehicles with largely decoupled dynamics that may be effectively treated even by elementary control methods. The most popular of these conventional multicopters is the four-propeller quadrotor, though six and eight propeller variants are seen in higher payload applications. Given their large thrust to weight ratios and a variety of control strategies, many interesting examples of body-fixed thrust vehicle capabilities have been demonstrated (e.g. Mellinger and Kumar (2011) and Lupashin et al. (2010)).

Despite their ubiquity, the maneuverability of these body-fixed thrust vehicles is fundamentally limited by the magnitude of the propeller reaction torque and the fact that only four of the vehicle's six degrees-of-freedom are actuated. Both of these issues may be addressed by actively directing the thrust with respect to the vehicle frame. In doing so, the pairwise arrangement of propellers may also be relaxed. The most straightforward implementation of this concept is the tricopter with three propellers, one of which may be tilted from vertical by way of a servo motor. Such a vehicle is described by Salazar-Cruz et al. (2009) and is well-known among multicopter hobbyists, since its four actuators may be manually steered by a pilot with a standard two-joystick (i.e. four-channel) remote control as in the body-fixed thrust vehicle case. The tilting action may be used to cancel the nominal non-zero reaction torque resulting from the odd number of propellers and, at the same time, enable comparatively high body yaw rates. The same behavior is realized by the tricopter design explored in Escareño et al. (2008) where all three propellers are slaved to tilt with the same angle. Propeller tilting may also be used to directly influence vehicle degrees of freedom that are not actuated in a conventional body-fixed thrust multicopter. This approach is taken by Ryll et al. (2014) where a quadrotor is described with four servos that independently tilt each of the four propellers. The arrangement of these eight actuators results in an ambiguous relationship between their configuration and the actuation of the vehicle's six-degrees-of-freedom. An online energy-minimizing optimization strategy is then used to uniquely determine the actuator configuration.

The present work describes a simpler yet just as capable vehicle with three independent tilting propellers. Their arrangement is chosen such that the six degrees-of-freedom of a single rigid body model of the vehicle is fully actuated with respect to the six vehicle inputs. These are assumed to be the three arm servo angles and the three propeller thrusts. In addition, a planar $2\pi/3$ arm distribution is chosen as to make lateral and longitudinal vehicle motions equally favorable. Ignoring the practical caveat of actuator saturation, the result is a vehicle capable of flying arbitrary trajectories. These include useful maneuvers unachievable by conventional body-fixed thrust multicopters such as

⋆ This work is supported in part by the German Research Foundation (DFG) in the framework of project "Regelung von Trikoptern beim gemeinsamen Transport von an Seilen aufgehängten Lasten".

10.1016/j.ifacol.2015.08.063

horizontal translation without tilting or hovering at an angle. The platform may likewise be used as a general purpose force and torque effector in three-dimensional space. The present results build upon the initial design and vehicle prototype established in Pillu (2012). While a similar vehicle was concurrently described by Mohamed and Lanzon (2012), no experimental results thereof were presented. This paper provides such results and a complete description of a pilot-supporting control scheme consisting of a nonlinear attitude tracking controller and a heading-referenced acceleration command generator.

1.1 Outline

This paper is organized as follows. Section 2 describes the vehicle geometry and the notation of its configuration. Models of the actuators and of the tricopter as a single rigid body mechanical model are discussed and equations of motion are presented. Finally, a brief sketch of a multi-body mechanical model of the system is included for later simulation. Section 3 outlines the pilot-supporting control approach and its main components: an attitude tracking controller and a heading-referenced acceleration command generator. Computation of the actuator inputs from the generalized body force is also covered. The implementation of the control scheme as well as a description of the vehicle's construction and electronic hardware is provided in Section 4. Finally, Section 5 demonstrates the performance of the attitude tracking controller for a test flight followed by conclusions and future work in Section 6.

2. MATHEMATICAL MODEL

A mathematical model of the tricopter forms the basis for the description of the vehicle's capabilities and the derivation of a suitable control scheme. In its derivation, a number of assumptions regarding the actuators and vehicle mechanics are made in the following. These are considered in the construction of the vehicle as will be discussed in Section 4, with ultimate justification thereof coming in the simulation and flight results presented in Section 5.

2.1 Vehicle geometry and configuration

The tricopter, as shown schematically in Figure 1, is made up of a central body and three motor-supporting arms, each supported by a revolute joint. The arm axes lie in a plane and are separated by an angle of $\frac{2\pi}{3}$. Their point of intersection $\mathcal{O}_b$ is taken as the origin of a right-handed axis system fixed to the central body and denoted by $\mathcal{B} = \{\boldsymbol{b}_1, \boldsymbol{b}_2, \boldsymbol{b}_3\} \subset \mathbb{R}^3$. The $\boldsymbol{b}_1$ and $\boldsymbol{b}_3$ axes are chosen as the direction of forward and vertical flight, respectively. The arms and their corresponding components are numbered starting opposite the positive $\boldsymbol{b}_1$ direction and increasing in a counter-clockwise sense about the $\boldsymbol{b}_3$ axis. The ith propeller rotation axis, denoted by $\boldsymbol{p}_{3i}$, is perpendicular to the ith arm axis and intersects the $\{\boldsymbol{b}_1, \boldsymbol{b}_2\}$ plane at a distance $\ell \in \mathbb{R}$ from $\mathcal{O}_b$. The centroid of the ith propeller is located a distance $h \in \mathbb{R}$ from the ith arm axis along $\boldsymbol{p}_{3i}$ and its revolute angle with respect to an arbitrary reference is denoted by $\psi_i \in \mathbb{R}$. The angle $\theta_i \in \mathbb{R}$ between $\boldsymbol{p}_{3i}$ and $\boldsymbol{b}_3$ is the ith propeller tilt angle with positive values taken in the counter-clockwise direction looking along the arm axis away from $\mathcal{O}_b$.

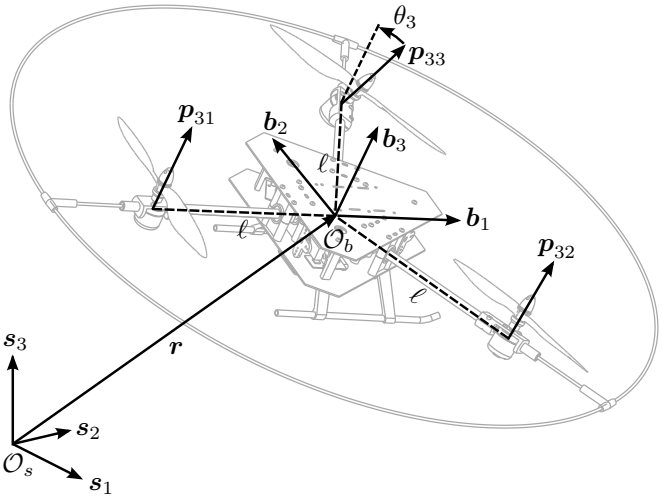

Fig. 1. Tricopter vehicle geometry and reference axes. The exemplary tilt angle of the 3rd propeller axis $\boldsymbol{p}_{33}$ with respect to body axis $\boldsymbol{b}_3$ is shown.

The configuration of the vehicle with respect to the (assumed inertial) spatial frame defined by origin $\mathcal{O}_s$ and right-handed orthogonal axes $\mathcal{S} = \{\boldsymbol{s}_1, \boldsymbol{s}_2, \boldsymbol{s}_3\} \subset \mathbb{R}^3$ is of interest. Here, $\boldsymbol{s}_3$ is parallel to the local gravity vector and $\{\boldsymbol{s}_1, \boldsymbol{s}_2\}$ is assumed to span the plane of the floor. The vehicle configuration is given by $(r, R) \in SE(3)$ where $r = [r^1, r^2, r^3]^\top \in \mathbb{R}^3$ is the column vector of coordinates of the vector $\boldsymbol{r} = \mathcal{O}_b - \mathcal{O}_s$ written in terms of the spatial frame directions [1] and $R \in SO(3)$ is the rotation matrix parameterizing the orientation of the body axes with respect to the spatial axes. That is, the jth column of R is given by $[\langle \boldsymbol{b}_j, \boldsymbol{s}_1\rangle, \langle \boldsymbol{b}_j, \boldsymbol{s}_2\rangle, \langle \boldsymbol{b}_j, \boldsymbol{s}_3\rangle]^\top$, where $\langle \cdot, \cdot \rangle$ denotes the inner product. The use of R to represent the vehicle attitude avoids the choice of a local parametrization (e.g. Euler angles) which is necessarily singular at some configuration.

2.2 Actuator model

Every revolute joint of the tricopter is actuated: servo motors set the joint angles and (feed-forward) speed-controlled motors set the propeller rotation rates. The aerodynamic effects of the resulting propeller movements are dominated by thrust and reaction torque production. For the ith propeller, their respective magnitudes are given by $f_{pi} = \kappa_F \dot{\psi}_i^2 \geq 0$ and $\tau_{pi} = -\epsilon_i \kappa_\tau \dot{\psi}_i^2$ and are assumed to act in the direction of $\boldsymbol{p}_{3i}$. Here, $\kappa_F > 0$ and $\kappa_\tau > 0$ are thrust and torque constants (assumed equal for all propellers) and $\epsilon_i = \pm 1$ describes the ith propeller's rotation sense with the positive value indicating a counter-clockwise sense about $\boldsymbol{p}_{3i}$. Further defining $\sigma := \frac{\kappa_\tau}{\kappa_F}$ allows for writing $\tau_{pi} = -\epsilon_i \sigma f_{pi}$, thereby clearly indicating the algebraic dependence between τ_{pi} and f_{pi}.

As a result, assuming that the dynamics of the underlying θ_i and $\dot{\psi}_i$, $i = 1, 2, 3$, controllers are negligible,

$$u = [f_{p1}, f_{p2}, f_{p3}, \theta_1, \theta_2, \theta_3]^\top \in \mathbb{R}^6 \tag{1}$$

may be taken as a column vector of independent vehicle inputs.

[1] i.e., $\boldsymbol{r} = \mathcal{O}_b - \mathcal{O}_s = \sum_{i=1}^{3} r^i \boldsymbol{s}_i$

2.3 Single rigid body mechanical model

The tricopter is approximated as a single rigid body for which the kinematics are given by

$$v = R^\top \dot{r} \tag{2a}$$
$$\dot{R} = R\,\widehat{\omega}. \tag{2b}$$

That is, $v \in \mathbb{R}^3$ and $\widehat{\omega} \in \mathfrak{so}(3)$ respectively represent the translational and rotational velocities of the body as expressed in the $\mathcal{B}$ axes. Note that $\widehat{\omega}$ is skew-symmetric (i.e., $\widehat{\omega}^\top = -\widehat{\omega}$) and related to $\omega = [\omega^1, \omega^2, \omega^3]^\top \in \mathbb{R}^3$ by

$$\widehat{\omega} = \begin{bmatrix} 0 & -\omega^3 & \omega^2 \\ \omega^3 & 0 & -\omega^1 \\ -\omega^2 & \omega^1 & 0 \end{bmatrix}.$$

In addition, define the so-called vee operator $(\cdot)^\vee : \mathfrak{so}(3) \to \mathbb{R}^3$ such that $(\widehat{\omega})^\vee = \omega$.

Assuming that $\mathcal{O}_b$ and the body's centre of mass are coincident, the vehicle's dynamics as expressed in the $\mathcal{B}$ axes is written as

$$m(\dot{v} + \widehat{\omega}\, v) = mR^\top g + f \tag{3a}$$
$$\Theta\,\dot{\omega} + \widehat{\omega}\,\Theta\,\omega = \tau. \tag{3b}$$

Here, $m \in \mathbb{R}_+$ and $\Theta \in \mathbb{R}^{3\times3}_{\succ 0}$ are the vehicle's mass and moment of inertia, respectively, $g = [0, 0, -9.81]^\top$ is the representation of the acceleration of gravity in $\mathcal{S}$, and $f \in \mathbb{R}^3$ and $\tau \in \mathbb{R}^3$ are the components of the forces and torques applied to the body. These final two quantities may be written together as $f_b := [f^\top, \tau^\top]^\top \in \mathbb{R}^6$ which is known as the generalized force for (3). The vehicle inputs u are related to f_b by the map $w\colon u \to f_b$ where

$$f_b = w(u) = W f_a \tag{4}$$

together with

$$W := \begin{bmatrix} 0 & 0 & 0 & 0 & \frac{\sqrt{3}}{2} & -\frac{\sqrt{3}}{2} \\ 0 & 0 & 0 & -1 & \frac{1}{2} & \frac{1}{2} \\ 1 & 1 & 1 & 0 & 0 & 0 \\ 0 & -\frac{\sqrt{3}}{2}\ell & \frac{\sqrt{3}}{2}\ell & 0 & -\frac{\sqrt{3}}{2}\epsilon_2\sigma & \frac{\sqrt{3}}{2}\epsilon_3\sigma \\ \ell & -\frac{1}{2}\ell & -\frac{1}{2}\ell & \epsilon_1\sigma & -\frac{1}{2}\epsilon_2\sigma & -\frac{1}{2}\epsilon_3\sigma \\ -\epsilon_1\sigma & -\epsilon_2\sigma & -\epsilon_3\sigma & \ell & \ell & \ell \end{bmatrix} \tag{5}$$

and

$$\begin{aligned} f_a := [&f_{p1}\cos\theta_1, f_{p2}\cos\theta_2, f_{p3}\cos\theta_3, \\ &f_{p1}\sin\theta_1, f_{p2}\sin\theta_2, f_{p3}\sin\theta_3]^\top. \end{aligned} \tag{6}$$

The determinant of the Jacobian matrix $\frac{\partial f_b}{\partial u} = W\frac{\partial f_a}{\partial u}$ is

$$\det\frac{\partial f_b}{\partial u} = \det W \det\frac{\partial f_a}{\partial u} > 0$$

since

$$\det W = \tfrac{3\ell}{4}\left(9\ell^2 + \sigma^2\sum_{i=1}^{3}\sum_{j=1}^{3}(3\delta_{ij}-1)\epsilon_i\epsilon_j\right) > 0, \tag{7}$$

given $\ell \gg \sigma > 0$, and

$$\det\frac{\partial f_a}{\partial u} = f_{p1}f_{p2}f_{p3} > 0, \tag{8}$$

so long as $f_{pi} > 0$, $i = 1, 2, 3$. As a result, w is an invertible map. Given this static one-to-one correspondence between input and generalized force, the tricopter with dynamics (3) may be said to be *fully actuated* by u.

2.4 Multi-body mechanical model

The single rigid body model of the tricopter presented in the previous section neglects a number of mechanical effects including

- offset between geometric body centre $\mathcal{O}_b$ and vehicle centre of mass resulting in coupled rotational and translation dynamics;
- the dependence of the vehicle centre of mass on arm and propeller angles;
- and mechanical coupling between arm and propeller rotation rates and overall vehicle dynamics.

In order to investigate the importance of such parasitic effects, a connected multi-body model is considered. The equations of motion thereof are derived via the energy-based approach from (Murray et al., 1994, Chapter 3–4) and briefly described in the following.

In addition to the central body, each arm is subdivided into two rigid bodies: the arm tube with motor stator; and the motor rotor with propeller. These two bodies are connected via a revolute joint, as is each arm to the central body. The configuration of the resulting seven-body system may be listed as the column vector $x := [z, s]^\top \in \mathbb{R}^{18}$ where[2] $z := [r^1, r^2, r^3, R^1_1, R^2_1, R^3_1, R^1_2, R^2_2, R^3_2, R^1_3, R^2_3, R^3_3]^\top$ and $s := [\theta_1, \theta_2, \theta_3, \psi_1, \psi_2, \psi_3]^\top$. Here, a distinction is made between the vehicle extrinsic quantities z and the intrinsic quantities s that parametrize its change in shape. Given the six constraints imposed on the entries of $R \in SO(3)$, the multi-body system has a total of $n = 12$ degrees-of-freedom, thus making x a redundant set of coordinates. A minimal parametrization of the rate of change of the vehicle's configuration is given by $\xi := [v^1, v^2, v^3, \omega^1, \omega^2, \omega^3, \dot\theta_1, \dot\theta_2, \dot\theta_3, \dot\psi_1, \dot\psi_2, \dot\psi_3] \in \mathbb{R}^{12}$. By expressing the kinetic energies of the bodies in terms of ξ and the potential energy of the vehicle in terms of x, the Lagrangian may be written. From there, Hamilton's principle of stationary action may be used to derive the equations of motion for the entire system subject to external forces. These take the form

$$M(s)\,\dot\xi + \mathrm{ad}^*_\xi M(s)\,\xi + c(s,\xi) = f_g(x) + f'_b(s,\xi) \tag{9}$$

where $M(s) \in \mathbb{R}^{12\times12}$ is the symmetric and positive definite mass matrix,

$$\mathrm{ad}^*_\xi = \begin{bmatrix} \mathrm{ad}^*_{\xi_z} & 0_{6\times6} \\ 0_{6\times6} & 0_{6\times6} \end{bmatrix} \quad \text{with } \mathrm{ad}^*_{\xi_z} = \begin{bmatrix} \widehat{\omega} & 0_{3\times3} \\ \widehat{v} & \widehat{\omega} \end{bmatrix},$$

$c(s,\xi) \in \mathbb{R}^{12}$ contains the so-called centrifugal and Coriolis forces, and $f_g(x) \in \mathbb{R}^{12}$ and $f'_b(s,\xi) \in \mathbb{R}^{12}$ are the generalized gravity and actuator forces, respectively. Due to the effects of the shape coordinates s, the expressions for the above quantities are extremely lengthy and are thus not given here. Their calculation is nonetheless useful in estimating the importance of parasitic mechanical effects via the simulation of (9) given physical vehicle parameters. Such a simulation will be carried out in Section 5.

3. CONTROL APPROACH

Manual pilot control of the fully actuated tricopter is not feasible. For one, the simultaneous command of the six

[2] $R^i_j \in \mathbb{R}$ is the (i,j)th entry of R.

components of the input u cannot be delivered by a conventional two-joystick radio remote control. Moreover, the relatively "fast" attitude dynamics of the vehicle present a significant physical challenge. Instead, an abstraction of the vehicle inputs is sought with which the pilot is presented a more natural command set suitable for a variety of flight trajectories. This so-called pilot-supporting controller is proposed in the following. This scheme is based on the approximate tricopter model (3) and is subdivided into attitude tracking control and heading-referenced acceleration command tasks by virtue of the decoupled translational and rotational dynamics. These subtasks respectively generate the generalized body force f_b command from which the vehicle inputs u are finally computed.

3.1 Attitude tracking controller

A attitude tracking controller based on (3b) is designed following Bullo and Murray (1999) and making specific use of Lemma 9 therein. A desired attitude and its rate of change are commanded. These are parametrized by $R_d \in SO(3)$ and $\omega_d = (R_d^\top \dot{R}_d)^\vee \in \mathbb{R}^3$, respectively. The deviation of the actual attitude from this reference may be described by $R_e \coloneqq R_d^\top R \in SO(3)$ with rate of change parametrized by $\omega_e = (R_e^\top \dot{R}_e)^\vee \in \mathbb{R}^3$. From these definitions, ω_d is represented in $\mathcal{B}$ as $\omega_{db} \coloneqq R_e^\top \omega_d$ and it follows that $\omega_e = \omega - \omega_{db}$ and thus

$$\dot{\omega}_e = \dot{\omega} - \dot{\omega}_{db}. \tag{10}$$

The attitude error dynamics is proposed:

$$\Theta\,\dot{\omega}_e + \widehat{\omega}_e\,\Theta\,\omega_e + K_D\,\omega_e + (\mathrm{Sk}\,(K_P\,R_e))^\vee = 0_3 \tag{11}$$

where $\mathrm{Sk}\,(R) = \frac{1}{2}(R - R^\top)$. By choosing $K_D \in \mathbb{R}^{3\times3}$ as positive definite and $K_P \in \mathbb{R}^{3\times3}$ as symmetric with eigenvalues $\{k_1, k_2, k_3\}$ such that $k_i + k_j > 0$ for $i \neq j$, it may be shown that the total rotational energy of the vehicle converges exponentially to zero from all initial conditions of R_e and ω_e. Substituting (10) and (11) into (3b) therefore yields the attitude controller

$$\tau = \Theta\,\dot{\omega}_{db} + \widehat{\omega}\,\Theta\,\omega - \widehat{\omega}_e\,\Theta\,\omega_e - K_D\,\omega_e - (\mathrm{Sk}\,(K_P\,R_e))^\vee. \tag{12}$$

The advantage of this rotation matrix-based control law over one relying on a local attitude parametrization is that it is not subject to singularities for specific orientations. The utility of such an attitude representation is particularly evident when highly-acrobatic trajectories are desired as discussed in Konz and Rudolph (2013).

3.2 Heading-referenced acceleration command

The pilot is tasked with the regulation of the translational tricopter dynamics which may be rewritten from (3a) as

$$f = m\,R^\top\,(\ddot{r} - g)\,.$$

The direct command of f, the body forces in $\mathcal{B}$, is impractical since R is free in general. Instead an alternative command variable is proposed, namely

$$a \coloneqq R_\gamma^\top\,\ddot{r} \in \mathbb{R}^3$$

where

$$R_\gamma = \begin{bmatrix} \cos\gamma & -\sin\gamma & 0 \\ \sin\gamma & \cos\gamma & 0 \\ 0 & 0 & 1 \end{bmatrix} \in SO(3) \tag{13}$$

and γ is the conventional ZYX-Euler yaw angle. As a result, a is the acceleration of the body in $\mathcal{S}$ as rotated about the local gravity vector in the direction of the vehicle's yaw angle. The body forces expressed in terms of a are given by

$$f = m\,R^\top\,(R_\gamma\,a - g)\,. \tag{14}$$

Compared to f, a is a natural command variable since its third component is always parallel to the local gravity vector and the remaining components may be inferred from the heading of the vehicle as seen by the pilot.

$m =$	1.23 kg
$\ell =$	0.2355 m
$\theta_i \in$	$[-55°, 55°]$
$[\epsilon_1, \epsilon_2, \epsilon_3] =$	$[+1, -1, -1]$
$\kappa_F =$	$1.42(10^{-5})$ Ns^2/rad^2
$\sigma =$	0.03 m

Table 1. Tricopter physical parameters.

3.3 Computing vehicle inputs

For a given instant, together (12) and (14) define the generalized body force f_b. Following the discussion in Section 2.3, a corresponding unique input u may be found. From (4)–(6), and considering (7)–(8) this inverse map is given by

$$f_a = W^{-1} f_b \tag{15}$$

and

$$f_{pi} = \sqrt{(f_a^i)^2 + (f_a^{i+3})^2} \tag{16a}$$

$$\theta_i = \mathrm{atan2}(f_a^{i+3}, f_a^i) \tag{16b}$$

for $i = 1, 2, 3$, where f_a^i denotes the ith component of f_a. It follows from (1) that u is thereby defined.

4. IMPLEMENTATION

The tricopter as described above and shown in Figure 2 has been constructed with an outside diameter of 0.75 m and an overall height of 0.115 m. Additional physical specifications are provided in Table 1. For rigidity, the central body and motor-supporting arms are constructed of carbon fibre plates and tubes, respectively. Each arm is supported by a pair of bearing blocks and actuated by a hobby servo via a single-bar linkage. The three 10"×4.5" propellers are driven by 110 W brushless outrunner motors equipped with (feed-forward) speed controllers. The high torque output of all six actuating motors justify the assumption that the arm angle and propeller rate dynamics may be neglected. Additionally, the lightweight arm construction and the distribution of the motor rotor and propeller above and below the arm axes serves to mitigate the parasitic mechanical coupling effects discussed in Section 2.4. Power is provided by a 2.4 Ah, 4S, lithium-polymer battery netting approximately 10 minutes of flight time.

All electronics are housed for protection between the central body plates. A VectorNav VN-100 inertial measurement unit (IMU) and attitude and heading reference system (AHRS) mounted at $\mathcal{O}_b$ and aligned with $\mathcal{B}$ provides the specific forces, angular rates, and orientation of the vehicle. An XBee radio modem enables for two-way data communication with a ground station computer and a standard digital 7-channel hobby receiver accepts pilot commands. All onboard computation is carried out

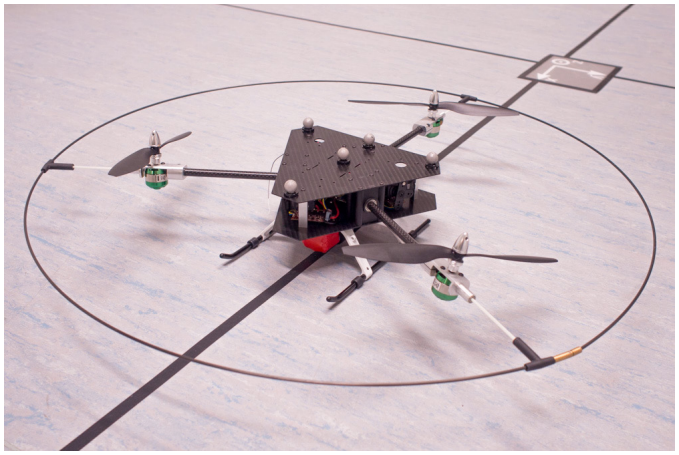

Fig. 2. Tricopter constructed at the Chair of Systems Theory and Control Engineering at Saarland University.

by a 66 MHz, 32-bit microcontroller with floating-point unit. The in-house developed firmware has a main loop frequency of 200 Hz.

4.1 Pilot-based control strategy

The pilot commands the tricopter by way of a 7-channel remote control. A single channel switch is used for enabling the vehicle, thus leaving six for motion commands. The tricopter maps three of the four channels assigned to the conventional two-joystick interface to a. The remaining joystick channel is interpreted as a commanded yaw angular rate which is integrated to produce a desired vehicle heading angle γ_d. Two sliders on the remote control are mapped to the desired roll and pitch angles α_d and β_d, respectively, and their corresponding rates of change are returned by a purposely-designed low-pass filter. The desired attitude and its rate of change are given by

$$R_d = \begin{bmatrix} \mathrm{c}\,\gamma_d \mathrm{c}\,\beta_d & \mathrm{c}\,\gamma_d \mathrm{s}\,\beta_d \mathrm{s}\,\alpha_d - \mathrm{s}\,\gamma_d \mathrm{c}\,\alpha_d & \mathrm{c}\,\gamma_d \mathrm{s}\,\beta_d \mathrm{c}\,\alpha_d + \mathrm{s}\,\gamma_d \mathrm{s}\,\alpha_d \\ \mathrm{s}\,\gamma_d \mathrm{c}\,\beta_d & \mathrm{s}\,\gamma_d \mathrm{s}\,\beta_d \mathrm{s}\,\alpha_d + \mathrm{c}\,\gamma_d \mathrm{c}\,\alpha_d & \mathrm{s}\,\gamma_d \mathrm{s}\,\beta_d \mathrm{c}\,\alpha_d - \mathrm{c}\,\gamma_d \mathrm{s}\,\alpha_d \\ -\mathrm{s}\,\beta_d & \mathrm{c}\,\beta_d \mathrm{s}\,\alpha_d & \mathrm{c}\,\beta_d \mathrm{c}\,\alpha_d \end{bmatrix}$$

and

$$\omega_d = \begin{bmatrix} -\mathrm{s}\,\beta_d \dot{\gamma}_d + \dot{\alpha}_d \\ \mathrm{s}\,\alpha_d \mathrm{c}\,\beta_d \dot{\gamma}_d + \mathrm{c}\,\alpha_d \dot{\beta}_d \\ \mathrm{c}\,\alpha_d \mathrm{c}\,\beta_d \dot{\gamma}_d - \mathrm{s}\,\alpha_d \dot{\beta}_d \end{bmatrix},$$

respectively, where $\mathrm{c} := \cos$ and $\mathrm{s} := \sin$. Such a configuration allows the pilot to set (α_d, β_d) in hover before navigating the environment by way of the two-joystick interface. Together, these pilot inputs define (a, R_d) which when combined with R and ω from the AHRS/IMU allow for the computation of f_b via (12) and (14). The corresponding actuator commands are subsequently calculated as described in Section 3.3 and sent to the servo motors and brushless motor speed controllers.

5. EXPERIMENTAL RESULTS

The performance of the vehicle and the described control approach is validated by an experiment denoted "Flight Trial 1" [3]. The attitude tracking performance of this 60 second flight is illustrated in Figure 3 and is good to within better than 2 degrees in most cases. Included therein are commanded periods of about −20, −12, and 10 degree roll angles beginning after 35 seconds. In order to provide an idea of the accompanying spatial trajectory of the vehicle body commanded by the pilot, its position as measured by a Vicon motion capture system is provided in Figure 4. Important to note is the apparent independence of the measured attitude and position trajectories when comparing Figures 3 and 4. This observation confirms the assumption that the rotational and translational are largely decoupled for this vehicle.

[3] video available at `http://www.uni-saarland.de/?trikopter`

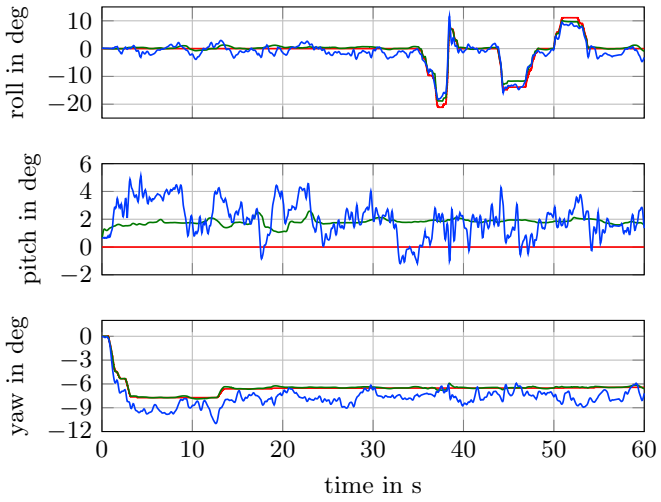

Fig. 3. Attitude tracking performance for "Flight Trial 1" in terms of ZYX-Euler angles. Their desired, experimentally measured, and simulated values are given in red, blue, and green, respectively.

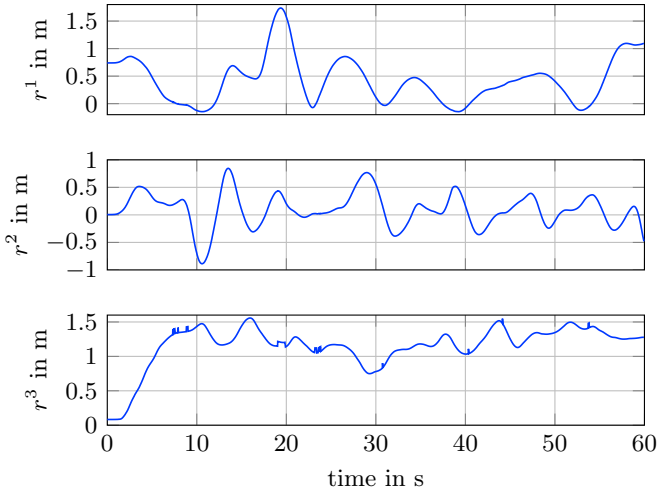

Fig. 4. Spatial position trajectory for "Flight Trial 1".

The simulation of the multi-body tricopter model (9) is also shown in Figure 3. This simulation is started with the actual measured attitude and driven by the recorded pilot remote control commands. One effect that is readily apparent from the simulation is the influence of the centre of mass offset from the vehicle's geometric centre on the pitch angle as observed experimentally. This offset was ignored in the derivation of the attitude controller and the resulting constant angle error cannot be entirely compensated by its proportional term. Finally, while a

number of the undesired transients seen in the attitude measurements are the result of wind turbulence in the small room where the flight test was conducted, further investigation into the actuator dynamics that were likewise neglected in the system model may be warranted.

6. CONCLUSION

A tricopter with three independent tilting propellers has been realized. The single rigid body model of the vehicle that neglects actuator dynamics has been shown to be valid for control design purposes. A pilot-supporting control scheme was described that provides a natural set of remote inputs for steering the vehicle even when tilted. This scheme is validated by flight test results that demonstrate good attitude tracking performance.

Future work involves the use of the Vicon measurements for position control. A geometric extension of the attitude controller used here is likewise provided by Bullo and Murray (1999) for this purpose. Additionally, the practical issue of actuator saturation must be treated. A starting point here may be the objective prioritization approach recently proposed by Hua et al. (2014).

ACKNOWLEDGEMENTS

The authors wish to acknowledge the contribution of the Research Internships in Science and Engineering (RISE) programme from the German Academic Exchange Service (DAAD) to the tricopter's practical realization. H. Pillu is also recognized for his instrumental work in realizing the first tricopter prototype as a visiting Master's student from Ecole Centrale de Lille.

REFERENCES

Bullo, F. and Murray, R.M. (1999). Tracking for fully actuated mechanical systems: a geometric framework. *Automatica*, 35(1), 17 – 34.

Escareño, J., Sanchez, A., Garcia, O., and Lozano, R. (2008). Triple tilting rotor mini-UAV: Modeling and embedded control of the attitude. In *American Control Conference, 2008*, 3476–3481. IEEE.

Hua, M.D., Hamel, T., and Samson, C. (2014). Control of VTOL vehicles with thrust-tilting augmentation. In *19th IFAC World Congress*, 2237–2244.

Konz, M. and Rudolph, J. (2013). Quadrotor tracking control based on a moving frame. In *Nonlinear Control Systems*, volume 9, 80–85.

Kumar, V. and Michael, N. (2012). Opportunities and challenges with autonomous micro aerial vehicles. *The International Journal of Robotics Research*, 31(11), 1279–1291.

Lupashin, S., Schöllig, A., Sherback, M., and D'Andrea, R. (2010). A simple learning strategy for high-speed quadrocopter multi-flips. In *Robotics and Automation (ICRA), 2010 IEEE International Conference on*, 1642–1648. IEEE.

Mellinger, D. and Kumar, V. (2011). Minimum snap trajectory generation and control for quadrotors. In *Robotics and Automation (ICRA), 2011 IEEE International Conference on*, 2520–2525.

Mohamed, M.K. and Lanzon, A. (2012). Design and control of novel tri-rotor UAV. In *UKACC International Conference on Control*, 304–309.

Murray, R.M., Li, Z., Sastry, S.S., and Sastry, S.S. (1994). *A mathematical introduction to robotic manipulation*. CRC press.

Pillu, H. (2012). *Conception, commande et contrôle d'un tricoptère*. Master's thesis, Ecole Centrale de Lille.

Ryll, M., Bilthoff, H., and Robuffo Giordano, P. (2014). A novel overactuated quadrotor unmanned aerial vehicle: Modeling, control, and experimental validation. *Control Systems Technology, IEEE Transactions on*, PP(99), 1–1. doi:10.1109/TCST.2014.2330999.

Salazar-Cruz, S., Lozano, R., and Escareño, J. (2009). Stabilization and nonlinear control for a novel trirotor mini-aircraft. *Control Engineering Practice*, 17(8), 886–894.